Chemical Geology 262 (2009) 100–107

Contents lists available at ScienceDirect

Chemical Geology

journal homepage: www.elsevier.com/locate/chemgeo

The density of volatile bearing melts in the Earth's deep mantle: The role of chemical composition

Zhicheng Jing *, Shun-ichiro Karato

Department of Geology and Geophysics, Yale University, P.O. Box 208109, New Haven, CT 06520, USA

ARTICLE INFO

Article history:
Accepted 24 February 2009

Keywords:
Silicate melts
Chemical composition
Water
Mg#
Density
Equation of state

ABSTRACT

Density of silicate melts in the Earth's deep interior is important to understand the material circulations in the mantle. We study the role of chemical composition on melt density based on the ideal-mixing model and the third-order Birch–Murnaghan equation of state (EOS). Using this EOS, the role of composition can be understood through its effect on three EOS parameters: room-pressure density, room-pressure bulk modulus, and the pressure derivative of bulk modulus at room pressure. The dependences of these parameters on compositional variables such as Mg# (molar MgO/(MgO + FeO) × 100) of the melt, SiO_2 content in the dry part of the melt, and H_2O content in the melt are estimated from available experimental data in the literature using the ideal-mixing model. Results show that H_2O content and Mg# of the melt are the most important factors that control the melt density at high pressure. Calculated densities of silicate melts are compared to the density of the ambient upper mantle from the PREM model near 410 km depth where dehydration-induced melting may occur. The relative density between the melt and the surrounding solid minerals is sensitive to the water content, Mg# and temperature at the conditions of melting. For an Mg# that is consistent with the pyrolite model, the conditions for density crossovers are marginally satisfied for a system when water (hydrogen) is the only volatile component to promote melting.

1. Introduction

Melting is one of the most important processes that control the chemical differentiation of the Earth. By melting, materials with different chemical compositions are created and then are separated by the gravity force. The density contrast between melts and residual solids determines the nature of this separation. Based on the observation that silicate liquids have significantly larger compressibilities than solids, Stolper et al. (1981) predicted that silicate melts might be denser than the surrounding solid residues in the deep upper mantle. If this density crossover between melts and solids occurs, then melts formed at high pressure may not be able to rise to the surface but instead will be trapped in the deep interior of the Earth. This will significantly modify our understanding of the chemical evolution of the Earth. This hypothesis has been shown to be valid for water-free systems (Agee and Walker, 1993; Suzuki et al., 1995; Suzuki and Ohtani, 2003).

However, the solidus temperature of a volatile-free system increases significantly with pressure, and therefore melting in the deep interior of the Earth likely occurs only with the help of some incompatible elements such as the volatile components (e.g., water). In the transition-zone water-filter model (hereafter referred to as the TZWF model) proposed by Bercovici and Karato (Bercovici and Karato, 2003; Karato et al., 2006), it is hypothesized that the melt formed by water-assisted melting could be denser than the upper mantle minerals (but lighter than the transition zone minerals) and hence will be trapped at the 410 km discontinuity. However, the validity of this assumption is not well established. Three recent experimental studies (Matsukage et al., 2005; Sakamaki et al., 2006; Agee, 2008) investigated the influence of water on the density of melts with various compositions. These studies have provided some constraints on the role of water to change the melt density at high pressure. However, in order to address the question of whether the melt formed at the 410 km discontinuity is denser than the upper mantle minerals, it is needed (i) to evaluate the influence of other chemical factors including the effect of FeO/MgO partitioning between melts and residue solids and the effect of other volatile elements and (ii) to evaluate the likely chemical composition of a melt formed at ~410 km depth. Karato et al. (2006) provided a rough estimate of the influence of other volatile elements. In the present paper, we will assume that the only volatile component is water and examine the influence of water and Mg# (molar MgO/(MgO + FeO) × 100).

Karato et al. (2006) showed that the influence of volatile component other than water is large and the conditions for the TZWF model to work may be limited. From the observational point of view, evidence for partial melting near 410 km depth is incomplete. On the one hand, there are some reports based on seismological observations that suggest the presence of partial melting at around 410 km in some regions (Revenaugh and Sipkin, 1994; Song et al., 2004). On the other

* Corresponding author. Tel.: +1 203 432 5791; fax: +1 203 432 3134.
E-mail address: zhicheng.jing@yale.edu (Z. Jing).

0009-2541/$ – see front matter © 2009 Elsevier B.V. All rights reserved.
doi:10.1016/j.chemgeo.2009.02.019

hand, there are some reports suggesting upwelling of materials from the transition zone (Booker et al., 2004; Zhao, 2004; Obayashi et al., 2006). It is possible that the conditions for a dense melt are satisfied in some cases but not always. Consequently, it is important to examine the details of the factors that affect the melt density under the conditions close to 410 km boundary.

Density of silicate melts depends on pressure, temperature, and composition. However, possible melt compositions in the deep Earth are poorly constrained. Therefore it is important to know how different melt components will influence the melt density. The effect of melt composition on density in the low pressure regime (up to 1–2 GPa) has been very well described by the ideal-mixing model (e.g., Bottinga and Weill, 1970; Lange and Carmichael, 1987). However, these results cannot be extrapolated to high pressure due to the assumed linear pressure dependence in their models.

At high pressure, the third-order Birch–Murnaghan equation of state (EOS) is widely used to describe the compression behavior of Earth materials including silicate melts. Recently, Jing a.nd Karato (2008) reviewed available melt density data in the literature determined from high-pressure sink/float experiments (Agee and Walker, 1988; Agee and Walker, 1993; Suzuki et al., 1995; Suzuki et al., 1998; Ohtani et al., 1998; Ohtani and Maeda, 2001; Suzuki and Ohtani, 2003; Matsukage et al., 2005; Sakamaki et al., 2006), and analyzed them using a normalized Birch–Murnaghan EOS with the constraints from room-pressure calibrations of melt density and bulk modulus. They showed that the pressure derivative of bulk modulus is basically independent of Mg#, but decreases with increasing SiO_2 content and H_2O content in the melts. In this study, we will combine these results with the results from the ideal-mixing model at room pressure to constrain the effects of chemical composition on melt density.

2. Effect of composition on density

In general, the density of silicate melts can be expressed as a function of pressure, temperature, and composition using an isothermal EOS,

$$\rho(P,T,X) = \rho(P;\rho_0(T,X),K_{T0}(T,X),K'_{T0}(T,X)\ldots \tag{1}$$

where the room-pressure density (ρ_0), the room-pressure bulk modulus (K_{T0}), and the pressure derivatives of bulk modulus at room pressure (K'_{T0},…) are temperature and compositional dependent parameters. Consequently, the influence of melt composition on density can be understood through the effect of composition on such EOS parameters. If we define C as an independent variable of the chemical composition of the melt, which could be the mole fraction of a melt component or a molar ratio of two different components, then a change in the compositional variable is δC. According to the chain rule of partial derivatives, the density change of the melt $\delta\ln\rho$ due to δC can be expressed as

$$\delta\ln\rho = \left(\frac{\partial\ln\rho}{\partial\ln\rho_0}\right)_{K_0,K'_{T0}}\frac{\partial\ln\rho_0}{\partial C}\delta C + \left(\frac{\partial\ln\rho}{\partial\ln K_{T0}}\right)_{\rho_0,K'_{T0}}\frac{\partial\ln K_{T0}}{\partial C}\delta C + \left(\frac{\partial\ln\rho}{\partial K'_{T0}}\right)_{\rho_0,K_{T0}}\frac{\partial K'_{T0}}{\partial C}\delta C \tag{2}$$

Consequently the calculation of the influence of composition on density can be separated into two steps: one is the effects of composition on EOS parameters, which are given by the partial derivatives $\frac{\partial\ln\rho_0}{\partial C}$, $\frac{\partial\ln K_{T0}}{\partial C}$, and $\frac{\partial K'_{T0}}{\partial C}$ and the other is the dependences of density on EOS parameters, which are given by the other three partial derivatives $\left(\frac{\partial\ln\rho}{\partial\ln\rho_0}\right)_{K_{T0},K'_{T0}}$, $\left(\frac{\partial\ln\rho}{\partial\ln K_{T0}}\right)_{\rho_0,K'_{T0}}$, and $\left(\frac{\partial\ln\rho}{\partial K'_{T0}}\right)_{\rho_0,K_{T0}}$. We will show in the following subsections that the first set of partial derivatives can be estimated from experimental data with the help of the ideal-mixing model, while the second set of partial derivatives can be derived from a specific formulation of EOS.

2.1. Dependences of density on EOS parameters

In this paper, we will use the Birch–Murnaghan EOS as an example of an isothermal EOS to demonstrate how density changes with changing EOS parameters. However, the method can be easily generalized to other forms of isothermal EOS such as the Vinet EOS. The third-order Birch–Murnaghan EOS is given by (Birch, 1947)

$$P = \frac{3}{2}K_{T0}\left[\left(\frac{\rho}{\rho_0}\right)^{7/3} - \left(\frac{\rho}{\rho_0}\right)^{5/3}\right]\left\{1 + \frac{3}{4}(K'_{T0}-4)\left[\left(\frac{\rho}{\rho_0}\right)^{2/3} - 1\right]\right\} \tag{3}$$

or in its normalized form

$$P^* = \frac{3}{2}\left[(\rho^*)^{7/3} - (\rho^*)^{5/3}\right]\left\{1 + \frac{3}{4}(K'_{T0}-4)\left[(\rho^*)^{2/3} - 1\right]\right\} \tag{4}$$

where

$$\rho^* = \rho(T,P,X)/\rho_0(T,X) \tag{5}$$

and

$$P^* = P/K_{T0}(T,X) \tag{6}$$

ρ_0, K_{T0}, and K'_{T0} are compositional dependent parameters that can be constrained by experimental data on melt densities and compressibilities.

Taking partial derivatives of Eq. (4) with respect to ρ_0, K_{T0}, and K'_{T0}, after some manipulation, the change in density due to a change in EOS parameters can be obtained as,

$$\left(\frac{\partial\ln\rho}{\partial\ln\rho_0}\right)_{K_{T0},K'_{T0}} = 1 \tag{7}$$

$$\left(\frac{\partial\ln\rho}{\partial\ln K_0}\right)_{\rho_0,K'_{T0}} = -\frac{P^*}{r} \tag{8}$$

$$\left(\frac{\partial\ln\rho}{\partial K'_{T0}}\right)_{\rho_0,K_{T0}} = -\frac{s}{r} \tag{9}$$

where

$$r = \frac{3}{2}\left[\frac{7}{3}(\rho^*)^{\frac{7}{3}} - \frac{5}{3}(\rho^*)^{\frac{5}{3}}\right] + \frac{9}{8}(K'_{T0}-4)\left[3(\rho^*)^3 - \frac{14}{3}(\rho^*)^{\frac{7}{3}} + \frac{5}{3}(\rho^*)^{\frac{5}{3}}\right] \tag{10}$$

and

$$s = \frac{9}{8}\left[(\rho^*)^3 - 2(\rho^*)^{\frac{7}{3}} + (\rho^*)^{\frac{5}{3}}\right] \tag{11}$$

It can be seen that $\left(\frac{\partial\ln\rho}{\partial\ln\rho_0}\right)_{K_{T0},K'_{T0}}$ is independent of pressure and equals 1. That is, 1% change in ρ_0 will result in 1% change in ρ, given K_{T0} and K'_{T0} fixed. On the contrary, $\left(\frac{\partial\ln\rho}{\partial\ln K_{T0}}\right)_{\rho_0,K'_{T0}}$ and $\left(\frac{\partial\ln\rho}{\partial K'_{T0}}\right)_{\rho_0,K_{T0}}$ are pressure dependent and have negative values. This is because an increase in K_{T0} or K'_{T0} will make the material less compressible at high pressure and hence will reduce the density. The absolute values of $\left(\frac{\partial\ln\rho}{\partial\ln K_{T0}}\right)_{\rho_0,K'_{T0}}$ and $\left(\frac{\partial\ln\rho}{\partial K'_{T0}}\right)_{\rho_0,K_{T0}}$ increase with increasing pressure. Given Eqs. (7)–(9), if we know how the EOS parameters vary with composition, that is, if we know the partial derivatives $\frac{\partial\ln\rho_0}{\partial C}$, $\frac{\partial\ln K_{T0}}{\partial C}$, and $\frac{\partial K'_{T0}}{\partial C}$, we will be able to predict the influence of melt composition on density.

2.2. Dependences of ρ_0 and K_{T0} on melt composition

ρ_0 as a function of composition is very well studied by the ideal-mixing model first proposed by Bottinga and Weill (1970) and later developed by many other studies including Lange (1997), Lange and Carmichael (1987), and Ochs and Lange (1997). In this model, the molar volume of a silicate melt is given by a linear combination of partial molar volumes of oxide components, viz.,

$$V_0 = \sum_i X_i \overline{V}_i \tag{12}$$

where X_i and $\overline{V}_i$ are the mole fraction and partial molar volume of the i-th component, respectively. Melt components are defined as the oxide components in melts such as MgO, SiO_2, H_2O, etc. The important feature of the ideal-mixing model is that $\overline{V}_i$ is independent of melt composition. Then the room-pressure density can be given by

$$\rho_0(T,X) = \frac{M}{V_0} = \frac{\sum_i X_i M_i}{\sum_i X_i \overline{V}_i} \tag{13}$$

where M and M_i are the total gram formula weight of the melt and the gram formula weight of the i-th component, respectively.

Mole fractions of the melt components seem to be a natural choice of compositional variables in order to obtain the partial derivatives like $\frac{\partial \ln\rho_0}{\partial C}$. However, X_i's are not independent of each other with the constraint,

$$\sum_i X_i = 1 \tag{14}$$

Therefore, it is more convenient to define independent variables of melt composition. Deep melts may have a broad range of compositions, including major components like SiO_2, Al_2O_3, FeO, MgO, CaO, and volatile components like H_2O, CO_2, Na_2O, and K_2O. Among all possible melt components, SiO_2, FeO, and MgO are the most interesting ones due to their high abundances in deep mantle melts. H_2O is another important melt component in the case of dehydration melting (Bercovici and Karato, 2003). We therefore define the independent compositional variables that are related to SiO_2, FeO, MgO, and H_2O as

$$C_M = \frac{X_{MgO}}{X_{MgO} + X_{FeO}} \times 100 \tag{15}$$

$$C_S = \frac{X_{SiO_2}}{1 - X_{H_2O}} \tag{16}$$

$$C_H = X_{H_2O} \tag{17}$$

That is, C_M is the Mg# of the melt, C_S is the mole fraction of SiO_2 in the dry part of the melt, and C_H is the mole fraction of H_2O in the melt. Compositional variables thus defined are independent of each other, that is, one variable can be changed without changing other variables. For example, if more H_2O is added to the melt, i.e., a change in C_H, Mg# (C_M) will remain the same, and vice versa. Other compositional variables such as mole fractions of CaO and Al_2O_3 in the dry part of the melt can also be defined. But these components are less important since they are less abundant in the deep melts. However, the method discussed here can be easily extended to theses components.

The compositional dependence of ρ_0 can be obtained by taking partial derivative of Eq. (13) with respect to the compositional variable C, which gives,

$$\frac{\partial \ln\rho_0}{\partial C} = \frac{\frac{\partial M}{\partial C} - \rho_0 \frac{\partial V_0}{\partial C}}{M} \tag{18}$$

where $\frac{\partial M}{\partial C}$ and $\frac{\partial V_0}{\partial C}$ can be obtained when the particular compositional variable C are defined as in Eqs. (15)–(17). Derivation results of $\frac{\partial M}{\partial C}$ and $\frac{\partial V_0}{\partial C}$ for $C = C_M$ are shown below; Results for other compositional variables are listed in Appendix A.

$$\frac{\partial M}{\partial C_M} = \left(M_{MgO} - M_{FeO}\right)\left(X_{MgO} + X_{FeO}\right) \tag{19}$$

$$\frac{\partial V_0}{\partial C_M} = \left(\overline{V}_{MgO} - \overline{V}_{FeO}\right)\left(X_{MgO} + X_{FeO}\right) \tag{20}$$

The change in ρ_0 due to a change in Mg# is then given by Eqs. (18)–(20).

In equations like Eqs. (19) and (20), the partial molar volumes $\overline{V}_i$ are required for the calculation. $\overline{V}_i$ has been calibrated by many studies. In this study we use the results of Lange (1997) for melt components other than FeO and H_2O. For the FeO component the result from Lange and Carmichael (1987) is used, and for H_2O the result from Ochs and Lange (1997) is used. Combining Eqs. (18)–(20), $\frac{\partial \ln\rho_0}{\partial C_M}$ can be calculated. Calculated results for all $\frac{\partial \ln\rho_0}{\partial C}$ that are interested in this study are shown in Table 1. The uncertainty in $\frac{\partial \ln\rho_0}{\partial C}$ comes from the uncertainty in $\overline{V}_i$, which is also reported in these calibrations. As an example the uncertainty in $\frac{\partial \ln\rho_0}{\partial C_M}$ can be obtained from error propagation as

$$\sigma^2_{\frac{\partial \ln\rho_0}{\partial C_M}} = \frac{\sigma^2_{\overline{V}_{MgO}} + \sigma^2_{\overline{V}_{FeO}}}{V_0^2}\left(X_{MgO} + X_{FeO}\right)^2 \tag{21}$$

where $\sigma_{\overline{V}_{MgO}}$ and $\sigma_{\overline{V}_{FeO}}$ are the uncertainties in $\overline{V}_{MgO}$ and $\overline{V}_{FeO}$, respectively.

Likewise, the compositional dependence of room-pressure bulk modulus K_{T0} can also be calculated using the ideal-mixing model of compressibility as,

$$\left(\frac{\partial V}{\partial P}\right)_0 = \sum_i X_i \frac{\partial \overline{V}_i}{\partial P} \tag{22}$$

Then K_{T0} is given by

$$K_{T0} = -V_0\left(\frac{\partial P}{\partial V}\right)_0 = -\frac{\sum_i X_i \overline{V}_i}{\sum_i X_i \frac{\partial \overline{V}_i}{\partial P}} \tag{23}$$

It should be noted that, the calculation of K_{T0} by the ideal-mixing model is an assumption. The physical picture for the mixing of melt components is not clear so there is no reason to believe that the ideal-mixing model is better than other models. However, Rivers and Carmichael (1987) and Ai and Lange (2008) have demonstrated that the ideal-mixing model used in this study (Eq. (22)) can reproduce experimental data on melt compressibility well.

Table 1
Composition dependences of EOS parameters[a].

Compositional variables C	$\frac{\partial \ln\rho_0}{\partial C}$	$\frac{\partial \ln K_{T0}}{\partial C}$	$\frac{\partial K'_{T0}}{\partial C}$
C_M	-0.00246 ± 0.00006	[b] 0.0021 ± 0.0002	0 ± 0.03
C_S	-0.377 ± 0.004	-0.81 ± 0.01	-10 ± 5
[c] C_H	-1.27 ± 0.02	-2.4 ± 0.3	-15 ± 10

[a] The temperature is assumed to be 1800 K for all calculations.
[b] For the temperature range that we are interested in (1800 K to 2000 K), most parameters vary only a few percent to around 10%. The only parameter that changes significantly is $\frac{\partial \ln K_{T0}}{\partial C_M}$, which changes from 0.0021 at 1800 K to 0.0036 at 2000 K. However, this will not significantly modify our results on the effect of Mg on melt density at high pressure because the absolute effect of Mg# on density through its effect on K_{T0} is small compared to its effect on ρ_0.
[c] The parameters for H_2O are only used in Fig. 1 to demonstrate that H_2O and Mg# are the most important factors that control melt density at high pressure. The quantitative results for effect of H_2O are calculated using an alternative approach as described in the text, i.e., using the experimentally determined partial molar volume of H_2O at high pressure.

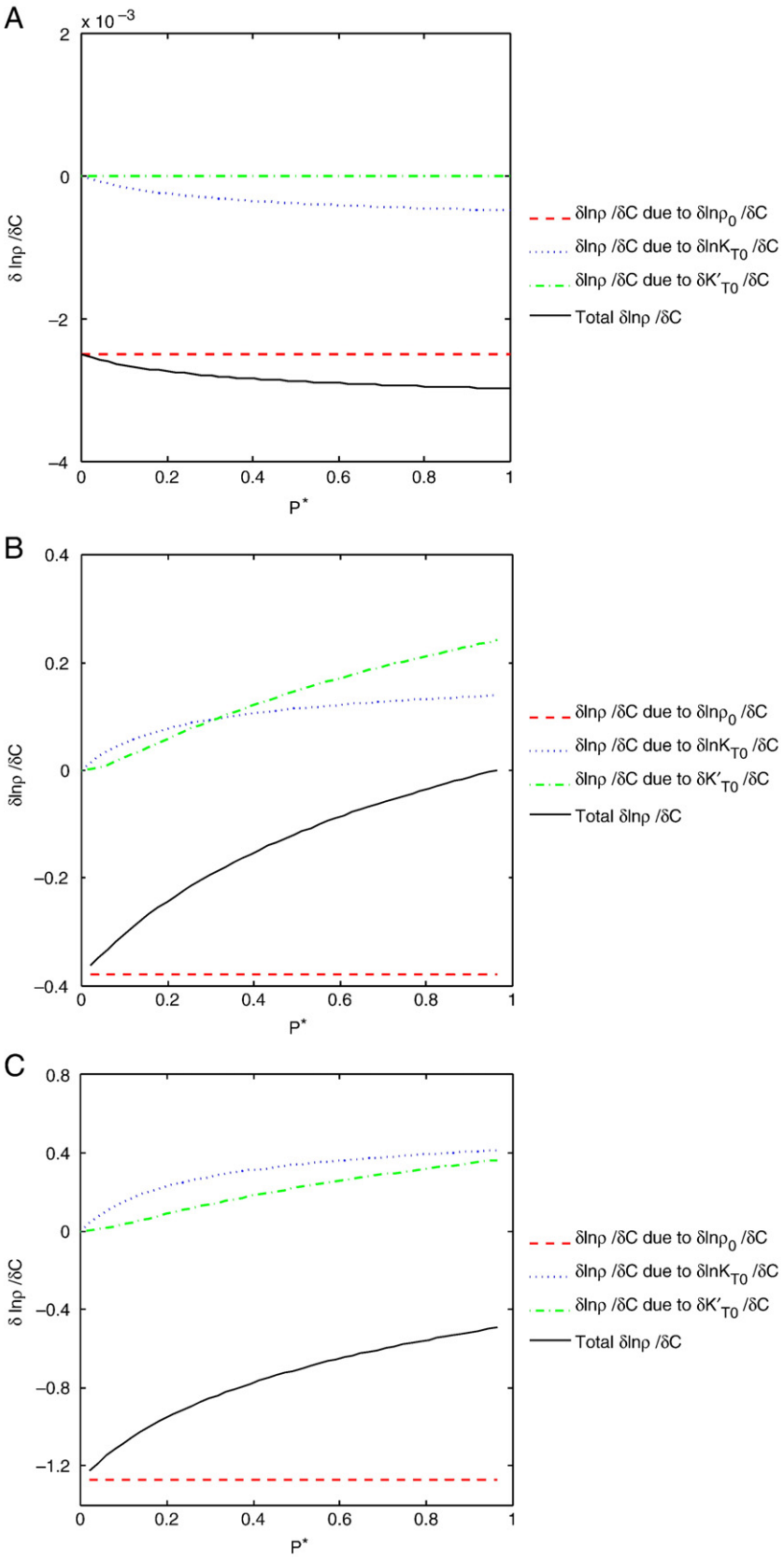

Fig. 1. Dependences of density on melt composition as a function of normalized pressure. Dashed curves, dotted curves, and dash-dotted curves are the density changes due to changes in ρ_0, K_{T0}, and K'_{T0}, respectively. Solid curves are the total changes in density due to the changes in all three EOS parameters. (A) The effect of C_M (Mg# of the melt); (B) The effect of C_S (mole fraction of SiO_2 in the dry part of the melt); (C) The effect of C_H (mole fraction of H_2O in the melt).

Taking partial derivative of Eq. (23) with respect to C, the compositional dependence of K_{T0} can be obtained as,

$$\frac{\partial \ln K_{T0}}{\partial C} = \frac{\frac{\partial V_0}{\partial C} + K_{T0}\frac{\partial}{\partial C}\left(\frac{\partial V}{\partial P}\right)_0}{V_0} \quad (24)$$

where $\frac{\partial V_0}{\partial C}$ and $\frac{\partial}{\partial C}\left(\frac{\partial V}{\partial P}\right)_0$ can be obtained when the particular compositional variable C is defined. Results of Eq. (24) for different compositional variables are shown in Appendix A.

When evaluating Eq. (24), calibrations of $\frac{\partial \overline{V}_i}{\partial P}$ are needed. For components of SiO_2, Al_2O_3, MgO, and CaO, $\frac{\partial \overline{V}_i}{\partial P}$ are given by the results of Ai and Lange (2008), which are based on the ultrasonic sound velocity studies of CaO–MgO–Al_2O_3–SiO_2 melts. For the FeO component, $\frac{\partial \overline{V}_i}{\partial P}$ is from the results of Kress and Carmichael (1991), which are based on the ultrasonic measurements of Fe-bearing melts. For the H_2O component, results based on the density estimation at elevated pressure from Ochs and Lange (1997) are used. Calculated results of $\frac{\partial \ln K_{T0}}{\partial C}$ with uncertainties are shown in Table 1.

2.3. Dependence of K'_{T0} on composition

Unlike ρ_0 and K_{T0}, K'_{T0} as a function of melt composition is not well determined. However, Jing and Karato (2008) recently analyzed available melt density data at high pressure obtained from sink/float experiments using a normalized Birch–Murnaghan EOS in combination with the room-pressure calibrations for ρ_0 and K_{T0}. In their approach, K_{T0} is calculated from the ideal-mixing model, therefore K'_{T0} is the only parameter to be constrained using high-pressure density data and the trade-off problem between K_{T0} and K'_{T0} is avoided. Consequently, the uncertainties in the fitted values of K'_{T0} are significantly reduced, and thereby the effect of composition on K'_{T0} can be resolved. They found that K'_{T0} is independent of Mg#, but decreases with increasing SiO_2 content. The presence of H_2O can also reduce K'_{T0} significantly. Given the results of Jing and Karato (2008), $\frac{\partial K'_{T0}}{\partial C_M}$, $\frac{\partial K'_{T0}}{\partial C_S}$, and $\frac{\partial K'_{T0}}{\partial C_H}$ are estimated to be 0 ± 3, -10 ± 5, and -15 ± 10 by linear regressions of the data in Fig. 2a, b, and c of Jing and Karato (2008). These results are listed in Table 1.

Given the influences of different compositional variables on ρ_0, K_{T0}, and K'_{T0}, we can summarize the effect of the Mg#, SiO_2 content in the dry part of the melt, and H_2O content on density in Fig. 1. Fig. 1A shows the change in density due to a change in Mg# at different pressures. Since FeO is a very dense component, substituting MgO with FeO will increase ρ_0 of the melts considerably. However, changing Mg# has no significant effects on K_{T0} and K'_{T0}. Therefore, the influence of Mg# on density comes mainly from its effect on ρ_0. Compared to FeO, SiO_2 can slightly decrease ρ_0 and K_{T0}, but can decrease K'_{T0} significantly due to its ability of changing coordination continuously with increasing pressure. The total density change due to changing SiO_2 content therefore is largely reduced to almost zero at high pressure (see Fig. 1B). H_2O also decreases all the EOS parameters ρ_0, K_{T0}, and K'_{T0}, similar to the effect of SiO_2, but to much larger extents. Therefore the overall effect of H_2O is to decrease the melt density, but this reduction in density diminishes with increasing pressures as a result of its effect on K_{T0} and K'_{T0} (see Fig. 1C). In a summary, MgO, FeO, SiO_2, and H_2O are the most abundant melt components in the deep mantle. Among these melt components, SiO_2 has a much smaller effect on melt density compared to Mg# and H_2O content. We will accordingly only consider the effect of Mg# and H_2O content on melt density in this study.

2.4. An alternative approach when the compositional dependence of K'_{T0} is not well constrained

Due to the limited number of density data at high pressure, $\frac{\partial K'_{T0}}{\partial C}$ may have very large uncertainties for some melt components like water, and may not be available for some other components. In these cases if we estimate the effect of composition on melt density based on Eq. (2), the uncertainty in $\frac{\partial K'_{T0}}{\partial C}$ would be too large to give any quantitative results. However, sometimes the partial molar volume of a melt component at high pressure can be estimated directly from experiments. For example, the partial molar volume of water at high pressure were estimated by several studies including Matsukage et al. (2005), Sakamaki et al. (2006), and Agee (2008); the partial molar volume of SiO_2 component was estimated up to 3.5 GPa by Gaetani et al. (1998). If the ideal mixing of partial molar volumes is still valid at high pressures, then using H_2O as an example, the density of the melt as a function of H_2O mole fraction can be estimated by the following equation,

$$\rho^{\text{melt}}(C_H) = \frac{(1 - C_H)M_{\text{dry}} + C_H M_{H_2O}}{(1 - C_H)V_{\text{dry}} + C_H \overline{V}_{H_2O}} \quad (25)$$

where M_{dry} and V_{dry} are the gram formula weight and the molar volume of the corresponding anhydrous melt. If the density of a hydrous melt is measured experimentally instead of the dry one, V_{dry} can be solved from Eq. (25) first, and then substituted back to give the density of hydrous melts as a function of C_H.

3. Conditions for density crossovers at the bottom of the upper mantle

3.1. Melt composition at 410 km depth

In the TZWF model, dehydration-induced partial melting is considered to occur above the 410 km boundary when upwelling mantle materials go across the phase transition boundary of wadsleyite and olivine. In order for the water filter to work, a gravitationally stable melt layer is required, that is, the melt layer must be denser than the surrounding materials in the upper mantle.

The composition of the melt formed at 410 km depth is not very well constrained. Matsukage et al. (2005) chose a target melt (hereafter referred to as the Mantle Melt) with 35.5 wt.% SiO_2, 3.3 wt.% Al_2O_3, 11.6 wt.% FeO, 30.4 wt.% MgO, 14.1 wt.% CaO, and 5 wt.% water as the melt composition at 410 km depth based on the hydrous melting experiments on CaO–MgO–Al_2O_3–SiO_2–pyrolite by Litasov and Ohtani (2002) and on CaO–MgO–FeO–Al_2O_3–SiO_2–pyrolite by Inoue and Sawamoto (1992). Based on high-pressure density measurements using the sink/float technique, the density of this melt at 14 GPa and 1800 K was then estimated to be 3.56 g/cm^3, which is higher then the density of the bottom of the upper mantle (3.54 g/cm^3) from the PREM model (Dziewonski and Anderson, 1981). In this study we will explore the conditions of melt-solid density crossover for a broader range of melt compositions. As we have shown in Section 2, the most important compositional variables that control melt density are mole fraction of H_2O (C_H) and Mg# (C_M) of the melt. Therefore we will test the TZWF model by modifying these two variables.

3.2. Effect of Mg# on melt density

Matsukage et al. (2005) determined the density of 4 hydrous ultramafic melts at 14 GPa and 1900 °C. These melts have the same H_2O content ($C_H = 0.134$) and SiO_2 content in the dry part of the melts ($C_S = 0.330$) as the Mantle Melt, but different Mg# ($C_M = 77$, 70, 63, and 61). Based on the method introduced in the previous section, we can estimate the effect of Mg# on melt density. Fig. 2 shows the calculated density as a function of Mg# of the melt together with the experimental data from Matsukage et al. (2005). It can be seen that the calculated density using the ideal-mixing model and the Birch–Murnaghan EOS are consistent with the experimental data.

For the melt above 410 km depth, the Mg# can be determined by studying the partitioning of Fe–Mg between the coexisting olivine

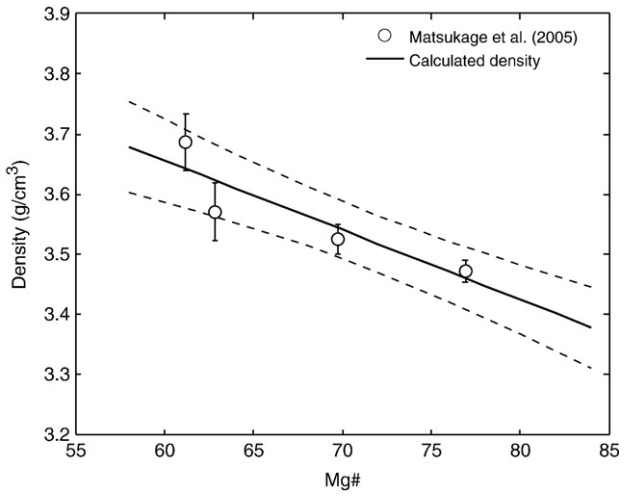

Fig. 2. Effect of Mg# on the density of melts at high pressure. H_2O content and SiO_2 content in the dry part of the melts are kept constant with $C_H = 0.134$ and $C_S = 0.330$. Circles are experimental data determined using sink/float experiments by Matsukage et al. (2005). The thick solid line is the calculated density as a function of Mg# with thin dashed lines as one standard deviation.

and melt that are in equilibrium. A distribution coefficient K_D is often defined as the ratio of Fe/Mg ratio in olivine to that in melt,

$$K_D = \frac{\left(X_{FeO}/X_{MgO}\right)^{olivine}}{\left(X_{FeO}/X_{MgO}\right)^{melt}} \tag{26}$$

K_D is estimated to be a constant value of 0.38 at high pressures according to Agee and Walker (1988). However a recent study using an improved experimental setup by Mibe et al. (2006) has shown that K_D at 410 km discontinuity could be as low as 0.25. This result is consistent with the observation of Kawamoto and Holloway (1997), in which they have shown that K_D decreases from 0.333 at 5 GPa to 0.258 at 11 GPa in the melting products of water saturated mantle peridotite. Therefore we will neglect the effect of H_2O on K_D. Smaller K_D means more FeO component will go to the melt instead of the MgO component and make the density crossover easier to occur.

Given K_D and the Mg# of olivine in the solid, Mg# of the melt can be obtained. Matsukage et al. (2005) assumed a rather high value of 92.5 for the Mg# of olivine at the bottom of the upper mantle. Then the Mg# of the mantle melt is estimated to be 82 if K_D is 0.38, but will be 76 if an updated K_D of 0.25 is used. However, the Mg# of olivine can be much smaller in the primitive mantle. Akaogi and Akimoto (1979) showed that the Mg# of olivine in the natural garnet lherzolite (PHN 1611), which has a similar composition as pyrolite, is about 87–88 at high pressures and is very close to the bulk Mg# of the system (also 87–88). It is therefore reasonable to believe that the Mg# of olivine in a more primitive region of the mantle can be similar to the bulk Mg# of 89 in the pyrolite model (Ringwood, 1966), and as a result the calculated Mg# of the melt will be 75 if K_D of 0.38 is used, and 67 if K_D of 0.25 is used.

3.3. Critical H_2O content for density crossovers at 410 km depth

Starting from the calculated melt density data at different Mg#s, we can expand the composition space further to a larger water content range. The density of the melts with a different H_2O content can then be estimated using Eq. (25) given the partial molar volume of water at high pressure.

Matsukage et al. (2005) estimated the partial molar volume of H_2O at 14 GPa and 2173 K is 8 ± 2 cm^3/mol. This result is consistent with other measurement by Agee (2008) and Sakamaki et al. (2006). By calculating the melt densities at different H_2O contents, the H_2O content at which the melt density equals the density of the upper mantle at 410 km depth is obtained. We hereafter refer to this H_2O content as the critical water content. Matsukage et al. (2005) noticed that the critical water content for density crossover to occur at 14 GPa highly depends on temperature. This is because that melt has a much larger coefficient of thermal expansivity than solid. Therefore with increasing temperature, the density of solid decreases a small amount, but the density of the melt decreases a larger extent. The critical water content can be obtained by the following equation,

$$\rho^{melt}_{T_m}(C_H)\exp(-\alpha_{melt}(T - T_m)) = \rho^{solid}_{T_s}\exp(-\alpha_{solid}(T - T_s)) \tag{27}$$

where T_m and T_s are the reference temperatures at which the density of the melt $\rho^{melt}_{T_m}$ and surrounding solids $\rho^{solid}_{T_s}$ are determined; α_{melt} and α_{solid} are the coefficients of thermal expansivity of the melt and solid at 14 GPa; C_H is the critical water content. For the melt, $\alpha_{melt} = 1.1\times10^{-4}K^{-1}$ is used based on the experimental result of Suzuki et al. (1998). For the solid, α_{solid} can be calculated from the relation of $\frac{\alpha}{\alpha_0} = \left(\frac{\rho}{\rho_0}\right)^{-\delta_T}$. If $\alpha_0 = 3\times10^{-5}K^{-1}$, $\rho_0 = 3.3$ g/cm^3, and the Anderson–Grüneisen parameter $\delta_T = 5.5$ (Fei, 1995), then we have $\alpha_{solid} = 2.1\times10^{-5}K^{-1}$.

The results of the critical water content for various Mg#s discussed above are shown in Fig. 4. It can be seen that at a higher temperature, the critical water content is smaller. The error propagation of Eq. (25) shows that the uncertainty in the critical water content comes mainly from the uncertainties in the partial molar volume of water and the uncertainties in thermal expansivity of melts. It should be noted that we have assumed that the ideal mixing of H_2O component is valid at high pressure, which otherwise will introduce some additional uncertainty. A recent study on hydrous $MgSiO_3$ melt with 10 wt.% H_2O by Mookherjee et al. (2008) showed an increasing of ideality of mixing of H_2O with increasing pressure as the partial molar volume of water in the melt approaches that of pure water. This nevertheless needs to be confirmed by direct experimental studies for hydrous melts with larger water contents up to 15 wt.%. The critical water content at 1800 K is about 14 wt.% given the updated K_D and Mg#,

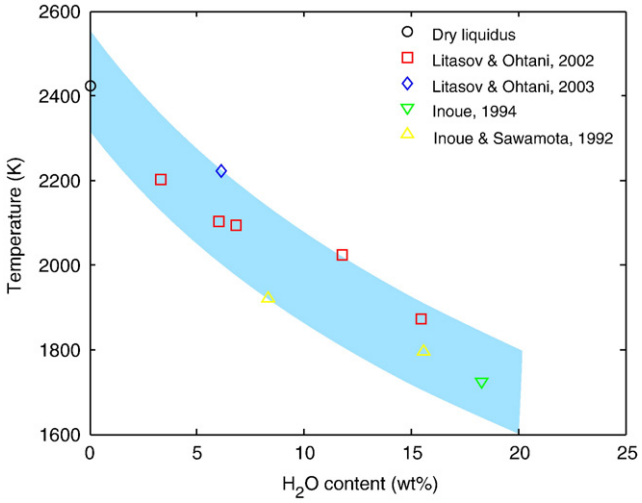

Fig. 3. Melting phase diagram (liquidus) for the pseudo-binary system of silicate–H_2O. Symbols are estimated water contents on the liquidus of the system from various experimental studies. The blue shaded area indicates the possible range of liquidus temperatures at different water content. (For interpretation of the references to colour in this figure legend, the reader is referred to the web version of this article.)

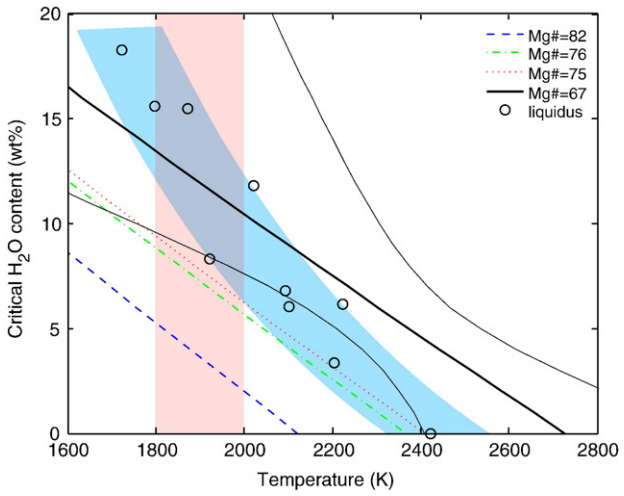

Fig. 4. Critical water content as a function of temperature for density crossovers between the melt and the upper mantle at 410 km depth. At a higher temperature the critical water content is smaller due to the larger thermal expansivity of the melt than that of the solid. The blue dashed line, green dash-dotted line, red dotted line, and the thick black solid line are for the melts that have Mg#s of 82, 76, 75, and 67, respectively. See text for detailed discussion of the Mg#. The thin black curves are estimated one standard deviation in the critical water content when the melt has an Mg# of 67. The orange shaded area indicates the possible range of temperature at 410 km. Also shown is the liquidus of the silicate-H_2O pseudo-binary system as circles and blue shaded area. Liquidus data are the same as those shown in Fig. 3. In the case that Mg# of the melt is 67, the conditions for density crossover at 410 km depth are marginally satisfied. (For interpretation of the references to colour in this figure legend, the reader is referred to the web version of this article.)

which is much higher than previously estimated value of ~6 wt.% in Matsukage et al. (2005).

4. Discussion

In the previous section, we have discussed the critical water content at which a melt can be denser than the surrounding upper mantle at 410 km depth at a range of temperature and Mg numbers. It is important to know if these conditions are accessible in the real Earth. From thermodynamics, the water content in the melt that is coexisting with the solid residues at different temperatures is given by the liquidus curve in the silicate–H_2O pseudo-binary system. With the addition of H_2O, the configurational entropy of the melt increases and hence the Gibbs free energy of the melt decreases. Therefore the presence of H_2O in the system lowers the melting temperature of the silicate. However, the liquidus curve in the silicate–H_2O system is not well constrained due to some experimental difficulties. One difficulty is that melts formed at these conditions are unquenchable, which makes the direct measurements of water contents in the melts very difficult. Also water may escape from quenched products once the sample charge is opened since the solubility of water in the quenched products is much lower at room pressure. Consequently only a few experimental data are currently available on the partial melt chemistry in the synthetic peridotite–H_2O system. Litasov and Ohtani (2002, 2003) determined the water content in the partial melts of the melting products of hydrous CaO–MgO–Al_2O_3–SiO_2–pyrolite by estimating electron microprobe totals of the quenched melts. However, this method could overestimate the water content in the melt since water might have escaped from melt during the quenching processes. Inoue (1994) determined the liquidus by studying the phase assemblages of the melting products directly. Although the starting material is a simple MgO–SiO_2–H_2O ternary system and the pressure is at 7.7 GPa, the results can still give a loose constraint since the liquidus temperature for the anhydrous system is less than 100 K different from that of mantle peridotite at 14 GPa. These constraints for the liquidus are shown in Fig. 3. Given the melting phase diagram, Fig. 4 also compares the critical water content with the water content at liquidus. It can be seen that for a melt that coexists with a pyrolite upper mantle (Mg# = 67 for the melt), the critical water content is slightly larger or overlap with the likely water content in the melt at the temperature of 410 km depth. Therefore conditions for density crossovers may be accessible in the real Earth, although the exact position of the liquidus curve is very critical.

It should be noted that in this study we have only considered water (hydrogen) as the impurity that causes the partial melting of the upper mantle atop the 410 km discontinuity. Other volatile components like CO_2, K_2O, and Na_2O can also be present in the melt as discussed in Karato et al. (2006). These volatile components may have larger densities in the melt than the H_2O component. Therefore, in the presence of these components the conditions for a gravitationally stable melt layer at 410 km discontinuity will be achieved at an even higher total volatile concentration in the melt.

5. Conclusions

The role of chemical composition on the density of hydrous silicate melts is studied using the third-order Birch–Murnaghan equation of state and the ideal-mixing model. Composition of the melts are described by independent compositional variables such as the Mg# of the melt, the SiO_2 mole fraction in the dry part of the melt, and the water content in the melt. Effects of these compositional variables are quantified by experimental data at both room pressure and high pressure. Results show that H_2O content and Mg# of melt are the most important parameters that control the melt density at high pressure. The conditions for density crossover between a hydrous ultramafic melt and the upper mantle at 410 km depth are constrained with an updated K_D value and Mg# of the melt. By comparing the critical water content with melting relations of the peridotite–H_2O pseudo-binary system, we conclude that for an Mg# that is consistent with the pyrolite model, the conditions for density crossovers are marginally satisfied. This suggests that filtering of incompatible elements by a dense melt proposed by Bercovici and Karato (2003) may work in some regions but not in other regions. It is important to study the role of other volatile components on melt density, on the one hand, and to investigate the regional variation in the nature of partially molten layer near the transition-zone from geophysical point of view, on the other hand.

Acknowledgements

This work was supported by the National Science Foundation. We thank anonymous reviewers for constructive comments.

Appendix A. Derivation of the compositional dependence of EOS parameters

As we have shown in the text, the compositional dependences of ρ_0 and K_{T0} can be derived in the framework of the ideal-mixing model (see Eqs. (13) and (23)). Once the independent compositional variables are defined as in Eqs. (15)–(17), the calculations of $\frac{\partial M}{\partial C}$, $\frac{\partial V_0}{\partial C}$, and $\frac{\partial}{\partial C}\left(\frac{\partial V}{\partial P}\right)_0$ in Eqs. (18) and (24) are straightforward. To simplify the derivation, we assume the melt has only four components, MgO, FeO, SiO_2, and H_2O. Then three independent variables of this system can be defined in Eqs. (15)–(17). Replacing the molar fractions of melt components by the independent compositional variables, we have,

$$M = M_{FeO} + \frac{1}{100}\left(M_{MgO} - M_{FeO}\right)C_M(1-C_S)(1-C_H) + \left(M_{SiO_2} - M_{FeO}\right)C_S(1-C_H) + \left(M_{H_2O} - M_{FeO}\right)C_H \quad \text{(A1)}$$

Taking partial derivative with respect to C_M, C_S, and C_H, after some manipulation, we have,

$$\frac{\partial M}{\partial C_M} = \frac{1}{100}\left(M_{MgO} - M_{FeO}\right)\left(X_{MgO} + X_{FeO}\right) \quad (A2)$$

$$\frac{\partial M}{\partial C_S} = \left(M_{SiO_2} - \frac{X_{MgO}M_{MgO} + X_{FeO}M_{FeO}}{X_{MgO} + X_{FeO}}\right)\left(1 - X_{H_2O}\right) \quad (A3)$$

$$\frac{\partial M}{\partial C_H} = M_{H_2O} - \frac{1}{1 - X_{H_2O}} \sum_{i \neq H_2O} X_i M_i \quad (A4)$$

Derivatives $\frac{\partial V_0}{\partial C}$ and $\frac{\partial}{\partial C}\left(\frac{\partial V}{\partial P}\right)_0$ have exactly the same function forms as $\frac{\partial M}{\partial C}$, except that M_i is replaced with $\overline{V_i}$ and $\frac{\partial \overline{V_i}}{\partial P}$, respectively. Although Eqs. (A2)–(A4) are derived by assuming only four components in the melt, the final results are the same for a system with more components.

References

Agee, C.B., 2008. Static compression of hydrous silicate melt and the effect of water on planetary differentiation. Earth and Planetary Science Letters 265, 641–654.

Agee, C.B., Walker, D., 1988. Static compression and olivine flotation in ultrabasic silicate liquid. Journal of Geophysical Research 93 (B4), 3437–3449.

Agee, C.B., Walker, D., 1993. Olivin flotation in mantle melt. Earth and Planetary Science Letters 114, 315–324.

Ai, Y., Lange, R.A., 2008. New acoustic velocity measurements on CaO–MgO–Al_2O_3–SiO_2 liquids: Reevaluation of the volume and compressibility of $CaMgSi_2O_6$–$CaAl_2Si_2O8$ liquids to 25 GPa. Journal of Geophysical Research 113, B04203.

Akaogi, M., Akimoto, S., 1979. High-pressure phase equilibria in a garnet lherzolite, with special reference to Mg^{2+}–Fe^{2+} partitioning among constituent minerals. Physics of the Earth and Planetary Interiors 19, 31–51.

Bercovici, D., Karato, S., 2003. Whole-mantle convection and the transition-zone water filter. Nature 425, 39–44.

Birch, F., 1947. Finite elastic strain of cubic crystals. Physical Review 71, 809–824.

Booker, J.R., Favetto, A., Pomposiello, M.C., 2004. Low electrical resistivity associated with plunging of the Nazca flat slab beneath Argentina. Nature 429, 399–403.

Bottinga, Y., Weill, D.F., 1970. Densities of liquid silicate systems calculated from partial molar volumes of oxide components. American Journal of Science 269, 169–182.

Dziewonski, A.M., Anderson, D.L., 1981. Preliminary reference Earth model. Physics of the Earth and Planetary Interiors 25, 297–356.

Fei, Y., 1995. Thermal expansion. In: Ahrens, T.J. (Ed.), Mineral Physics & Crystallography a Handbook of Physical Constants. AGU, pp. 29–41.

Gaetani, G.A., Asimow, P.D., Stolper, E.M., 1998. Determination of the partial molar volume of SiO2 in silicate liquids at elevated pressures and temperatures: a new experimental approach. Geochimica et Cosmochimica Acta 62, 2499–2508.

Inoue, T., 1994. Effect of water on melting phase relations and melt composition in the system Mg_2SiO_4–$MgSiO_3$–H_2O up to 15 GPa. Physics of the Earth and Planetary Interiors 85, 237–263.

Inoue, T., Sawamoto, H., 1992. High pressure melting of pyrolite under hydrous condition an its geophysical implications. In: Syono, Y., Manghnani, M.H. (Eds.), High-pressure Research: Application to Earth and Planetary Sciences. American Geophysical Union, Washington, D. C., pp. 323–331.

Jing, Z., Karato, S., 2008. Compositional effect on the pressure derivatives of bulk modulus of silicate melts. Earth and Planetary Science Letters 272, 429–436.

Karato, S., Bercovici, D., Leahy, G., Richard, G., Jing, Z., 2006. The transition-zone water filter model for global material circulation: where do we stand? In: Jacobsen, S.D., van der Lee, S. (Eds.), Earth's Deep Water Cycle. American Geophysical Union, Washington, DC, pp. 289–313.

Kawamoto, T., Holloway, J.R., 1997. Meting temperature and partial melt chemistry of H_2O-saturated mantle peridotite to 11 gigapascals. Science 276, 240–243.

Kress, V.C., Carmichael, I.S.E., 1991. The compressibility of silicate liquids containing Fe_2O_3 and the effect of composition, temperature, oxygen fugacity adn pressure on their redox states. Contributions to Mineralogy and Petrology 108, 82–92.

Lange, R.A., 1997. A revised model for the density and thermal expansivity of K_2O–Na_2O–CaO–MgO–Al_2O_3–SiO_2 liquids from 700 to 1900 K: extension to crustal magmatic temperatures. Contributions to Mineralogy and Petrology 130, 1–11.

Lange, R.A., Carmichael, I.S.E., 1987. Densities of Na2O–K2O–CaO–MgO–FeO–Fe_2O_3–$A1_2O_3$–TiO_2–SiO_2 liquids: new measurements and derived partial molar properties. Geochimica et Cosmochimica Acta 51, 2931–2946.

Litasov, K., Ohtani, E., 2002. Phase relations and melt compositions in CMAS–pyrolite–H_2O system up to 25 GPa. Physics of the Earth and Planetary Interiors 134, 105–127.

Litasov, K., Ohtani, E., 2003. Hydrous solidus of CMAS–pyrolite and melting of mantle plumes at the bottom of the upper mantle. Geophysical Research Letters 30 (22), 2143. doi:10.1029/2003GL018318.

Matsukage, K.N., Jing, Z., Karato, S., 2005. Density of hydrous silicate melt at the conditions of Earth's deep upper mantle. Nature 438, 488–491.

Mibe, K., Fujii, T., Yasuda, A., Ono, S., 2006. Mg–Fe partitioning between olivine and ultramafic melts at high pressure. Geochimica et Cosmochimica Acta 70, 757–766.

Mookherjee, M., Stixrude, L., Karki, B., 2008. Hydrous silicate melt at high pressure. Nature 452, 983–986.

Obayashi, M., Sugioka, H., Yoshimitsu, J., Fukao, Y., 2006. High temperature anomalies oceanward of subducting slabs at the 410-km discontinuity. Earth and Planetary Science Letters 243, 149–158.

Ochs, F.A., Lange, R.A., 1997. The partial molar volume, thermal expansivity, and compressibility of H2O in NaAlSi3O8 liquid: new measurements and an internally consistent model. Contributions to Mineralogy and Petrology 129, 155–165.

Ohtani, E., Maeda, M., 2001. Density of basaltic melt at high pressure and stability of the melt at the base of the lower mantle. Earth and Planetary Science Letters 193, 69–75.

Ohtani, E., Suzuki, A., Kato, T., 1998. Flotation of olivine and diamond in mantle melt at high pressure: implications for fractionation in the deep mantle and ultradeep origin of diamond. Properties of Earth and Planetary Materials at High Pressure and Temperature. American Geophysical Union, pp. 227–238.

Revenaugh, J., Sipkin, S.A., 1994. Seismic evidence for silicate melt atop the 410 km mantle discontinuity. Nature 369 (6480), 474–476.

Ringwood, A.E., 1966. Mineralogy of the mantle. In: Hurley, P.M. (Ed.), Advances in Earth Science. M.I.T. Press, Cambridge, MA, pp. 357–399.

Rivers, M.L., Carmichael, I.S.E., 1987. Ultrasonic studies of silicate melts. Journal of Geophysical Research 92 (B9), 9247–9270.

Sakamaki, T., Suzuki, A., Ohtani, E., 2006. Stability of hydrous melt at the base of the Earth's upper mantle. Nature 439, 192–194.

Song, T.-R.A., Helmberger, D.V., Grand, S.P., 2004. Low-velocity zone atop the 410-km seismic discontinuity in the northwestern United States. Nature 427, 530–533.

Stolper, E., Walker, D., Hager, B.H., Hays, J.F., 1981. Melt segregation from partially molten source regions: the importance of melt density and source region size. Journal of Geophysical Research 86 (B7), 6261–6271.

Suzuki, A., Ohtani, E., 2003. Density of peridotite melts at high pressure. Physics and Chemistry of Minerals 30, 449–456.

Suzuki, A., Ohtani, E., Kato, T., 1995. Flotation of diamond in mantle melt at high pressure. Science 269, 216–218.

Suzuki, A., Ohtani, E., Kato, T., 1998. Density and thermal expansion of a peridotite melt at high pressure. Physics of the Earth and Planetary Interiors 107, 53–61.

Zhao, D., 2004. Global tomographic images of mantle plumes and subducting slabs: insight into deep Earth dynamics. Physics of the Earth and Planetary Interiors 146, 3–34.